PCCP

Accepted Manuscript

ROYAL SOCIETY OF CHEMISTRY

www.rsc.org/pccp

Journal Name

ARTICLE

Phase transition kinetics and surface binding states of methylammonium lead iodide perovskite

Received 00th January 20xx,
Accepted 00th January 20xx

DOI: 10.1039/x0xx00000x

www.rsc.org/

G. Rajendra Kumar[a], A. Dennyson Savariraj[a], S. N. Karthick[a], S. Selvam[a], B. Balamuralitharan[a], Hee-Je Kim[a], K.K. Viswanathan[b], M. Vijaykumar[c], Kandasamy Prabakar*[a,c]

We have presented a detailed analysis of phase transition kinetics and binding energy states of solution processed methylammonium lead iodide ($MAPbI_3$) thin films prepared at ambient conditions and annealed at different elevated temperatures. The processing temperature and environmental conditions predominantly control the crystal structure and surface morphology of $MAPbI_3$ thin films. The structural transformation from tetragonal to cubic occurs at 60°C for 30 minutes annealing time while 10 minutes annelaed films posses tetragonal crystal structure. The transformed phase is greatly intact even at higher annealing temperature of 150 °C and time of 2 hours. The charge transfer interaction between Pb 4f and I 3d oxidation state is quantified by the XPS.

1. Introduction

World's energy consumption is moving towards the renewable energy resources, mainly the solar energy due to environmental concern related to global warming and sustainability. The challenge has always been in the conversion of solar energy into an electrical energy with efficient and cost-effective way. Though, crystalline silicon dominates the photovoltaic industry with efficiencies over 20%, it remains relatively expensive to manufacture.[1] In silicon photovoltaics, the substantial reduction of manufacturing cost is highly required to assure the mass production and fulfil future energy consumption demand.[2] Recently, single or multiple solution processes have been introduced to fabricate dye-sensitized,[3] quantum dot,[4] and polymer solar cells[5] at low temperature and the manufacturing cost of the cells are cheaper than silicon cells; however, they still suffer from long-term stability and low power conversion efficiency (PCE) as a result of fundamental energy losses occurring at heterojunction interface.[6]

Perovskite solar cells have emerged as a leader of the photovoltaic technology and it seems to contribute large scale solar energy production due to its high PCE and compatibility with scalable processes are promising an alternative to conventional silicon solar cells.[7] Especially, the $MAPbI_3$ perovskite light harvester having the direct band gap of about 1.45–1.6 eV, high carrier mobility, large absorption coefficients and ability to form very high quality crystals rapidly at low temperature are added advantages.[8]

The introduction of $MAPbI_3$ as a sensitizer in an electrolyte based dye-sensitized solar cells (DSSCs) is marked as the beginning of perovskite-based photovoltaic technology.[9] Consequently, the planar heterojunctions and mesoscopic metal oxide structured solar cells boot with higher concert.[10] Since the first work published on $MAPbI_3$ perovskite, a set of prominent ideas stimulated over past few years with different feasible methodologies focused only to achieve higher efficiency, but lacks on identifying the cause of perovskite degradation when exposed to the air.[11, 12]

The hygroscopic nature of methylammonium (MA) cation traps the moisture from the air which increases the crystal size along with contamination. However, moisture is not the only problem for degradation, even the perovskite devices processed in inert (N_2) atmosphere also undergoes destabilization.[12, 13] Device interface may also play a crucial role in degradation mechanism.[14] This issue has grown as a big concern to fabricate perovskite-based photovoltaic devices in large scale. It is mainly due to the lack of understanding their physical properties. In this work, we have intensely focused to investigate the phase transition kinetics and surface binding states of $MAPbI_3$ thin films prepared at ambient conditions and processed at different temperatures such as 60 °C, 100 °C, and 150 °C and tried to understand the real issues instigated on the perovskite over the fundamental physical properties beyond the concern of photovoltaic efficiency. Here, we report the $MAPbI_3$ thin film prepared on Fluorine doped tin oxide (FTO) substrate under atmosphere. It is highly challenging task to make the uniform coverage of perovskite film on FTO by the spin coating at ambient atmosphere. Accordingly, we optimized the parameters such as concentration of both methylammonium iodide (MAI) and lead iodide (PbI_2), utilized different solvents based on their dielectric constant, spin speed with respect to the number of layers deposited, annealing time and temperature helped us to achieve uniform film coverage with stability. Subsequently, the samples were employed for different physical characterizations to examine the quality of film through the structural and morphological properties. The phase transition occurs at 60 °C for

[a] Department of Electrical and Computer Engineering, Pusan National University, San 30, Jangjeong-Dong, Gumjeong-Ku, Busan-609 735, South Korea
[b] UTM Centre for Industrial and Applied Mathematics,Ibnu SIna Institute for Scientifc & Industrial Research, Department of Mathematical Sciences, Faculty of Science, Universiti Teknologi Malaysia, 81310, Johor Bahru, Johor, Malaysia.
[c] Pacific Northwest National Laboratory (PNNL), Richland, WA-99354, USA

† Electronic Supplementary Information (ESI) available: William-Hall Plot for estimation of grain size and lattice strain of $MAPbI_3$ films, XPS survey spectra with elemental concentration, Estimation of atomic percentage of C 1s, O 1s, and N 1s using AM-RSFs method. See DOI: 10.1039/x0xx00000x

the films annealed for 30 minutes and the noticeable changes in the binding states according to atmospheric effects are discussed in this work.

2. Experimental

2.1 Preparation of $MAPbI_3$ thin film

The FTO substrates (7-10 Ω cm^{-1}, Hartford Glass Corporation) were well-cleaned sequentially in an ultrasonic bath with ethanol, acetone and deionized water for 10 minutes followed by drying under N_2 gas. All chemicals were purchased from Sigma Aldrich and used as received unless otherwise stated. The $MAPbI_3$ perovskite precursor was prepared by dissolving 2:1 molar ratio of MAI and PbI_2 in N, N-dimethylformamide (DMF) under stirring at 60 °C for overnight. The $MAPbI_3$ precursor solution was drop casted on FTO for three consecutive cycles at an optimized spin speed of 2000 rpm for 30 s. After spin coating, each set of films were annealed at 60 °C, 100 °C and 150 °C in air for 10, 30, 60 and 120 minutes.

2.2 Characterization

The phase identification of the spin-coated $MAPbI_3$ perovskite films were analysed by X-ray diffraction (XRD; Bruker D8-Advance) with Cu Kα radiation (λ = 1.540Å) source operated at 40 kV and 30 mA in the range 10–60°. UV-visible spectroscopy was performed by using an Optizen 3220 UV spectrophotometer in the 400-800 nm wavelength range. The morphology of the films was observed using a field-emission scanning electron microscopy (FE-SEM) (Hitachi, model S-4200) operated at 15 kV, 150W. X-ray photoelectron spectroscopy (XPS) was performed using a Thermo Fisher Scientific (U.K) ESCALAB 250 system with monochromatic Al Kα radiation of 1486.6 eV and with an electron take off angle of 45°. The measurement was conducted without ion etching, to avoid reconfiguration of the bonds. The pressure of the chamber was kept at 10^{-10} Torr during the measurement. The survey spectrum was scanned in the binding energy (BE) range 100 - 1200 eV in steps scan of 1 eV with spot size 500 μm. All of the obtained binding energy is compensated with the core level peak of adventitious carbon (C 1s) at 284.6 eV, fixed as a reference. We used the lowest possible number of components to fit the data satisfactorily. The uncertainty in binding energy position was within 0.05 eV for a particular component. Peak fitting and quantitative analysis were done using Casa XPS program (Casa Software Ltd) and the results were justified by average matrix relative sensitivity factor (AM-RSF) with respect to peak area and atomic sensitivity factor of the identified components. The binding energy of the identified components was assigned from NIST X-ray Photoelectron Spectroscopy Database (NIST Standard Reference Database 20, Version 4.1).

3. Results and discussion

3.1 Structural analysis

XRD analysis was carried out to understand the effect of temperature on structural properties of $MAPbI_3$ films processed in atmospheric conditions. Figure 1(a) shows the XRD for the $MAPbI_3$ films annealed at 60 °C, 100 °C and 150 °C for 10 minutes. The diffraction peaks of FTO at 26.52, 33.67, and 37.75° are assigned to (222), (314), (200) lattice planes. The $MAPbI_3$ thin films have preferential orientation with a=8.789Å and c=12.567Å axis for tetragonal perovskite structure at RT with (110), (202), (220), (310), (224), (314), (330) lattice planes

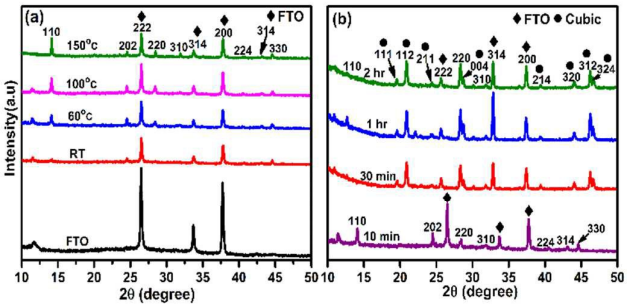

Figure 1. X-ray diffraction spectra of $MAPbI_3$ perovskite film at (a) RT and annealed at 60 °C, 100 °C, and 150 °C for 10 minutes (b) annealed at 60 °C for 10, 30,60 and 120 minutes.

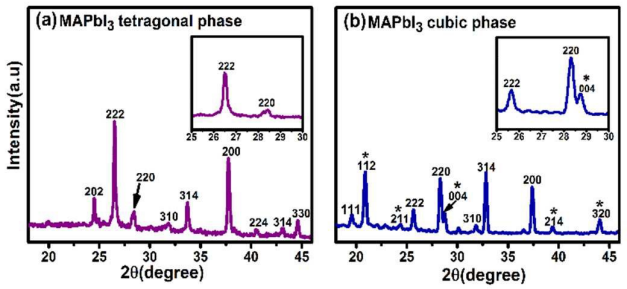

Figure 2. XRD spectra of $MAPbI_3$ thin films annealed at 60 °C for (a) 10 minutes (tetragonal) b) 30 minutes (cubic). Inset show the splitting of diffraction peak.

corresponding to 14.10, 24.5, 28.50, 31.87, 40.55, 43.17 and 44.60° (2θ) diffraction positions respectively.[15, 16] The indexing was performed by the relative combination of planar-spacing and Bragg's law, which determine the unit cell parameters from the peak positions.[17, 18] The intensity of $MAPbI_3$ characteristic peaks gradually raised with reduced full width at half maximum when annealing temperature is increased along with few peaks disappeared and new minor peaks appear at 150 °C due to elimination of defects. The substantial changes in the $MAPbI_3$ perovskite crystal structure from tetragonal to cubic occurs at 60 °C through unit cell distortion and maintained the crystal structure even at 150 °C with increased grain size. Figure 1(b) shows XRD spectra of $MAPbI_3$ thin films annealed at 60 °C for 30, 60 and 120 minutes. Even though, the crystal growth has been initiated at RT itself, the film structure is significantly reformed at 60 °C annealed for 30 minutes. It is observed that shifting of $MAPbI_3$ characteristic peaks occur towards the lower angles and new peaks appear at (111), (112), (004), (312), (324) lattice planes corresponding to 19.59, 20.85, 28.80, 46.24, 46.75°(2θ) positions respectively. The diffraction peak of (220) split into (004) and (220) crystal planes for the films annealed at 60 °C for 30 minutes indicates the structural transformation of $MAPbI_3$ from the tetragonal to cubic crystal structure[19] and is shown in Figure 2. However, there is no significant change in the crystal structure is observed even when the annealing time is increased up to 120 minutes at 60 °C. The parallel results are obtained for the higher annealing temperatures of 100 °C and 150

°C as is shown in Figure 3. The phase transformation of perovskite from tetragonal to cubic is schematically represented in Figure 4. The transformed phase is highly conserved at longer annealing time of 120 minutes and higher annealing temperature of 150 °C. The phase transition of perovskite is mainly due to its low tolerance factor of 0.83 and the alteration of $d_{spacing}$ upon annealing.[8] The tetragonal crystal structure exhibited below 60 °C is distorted by the thermal vibration of lattice planes upon annealing by the rotational disorder of MA^+ ions due to short relaxation and the atomic disordering of iodide (I) ions which may decrease or increase its symmetry in the way of expanded or contracted.[20, 21]

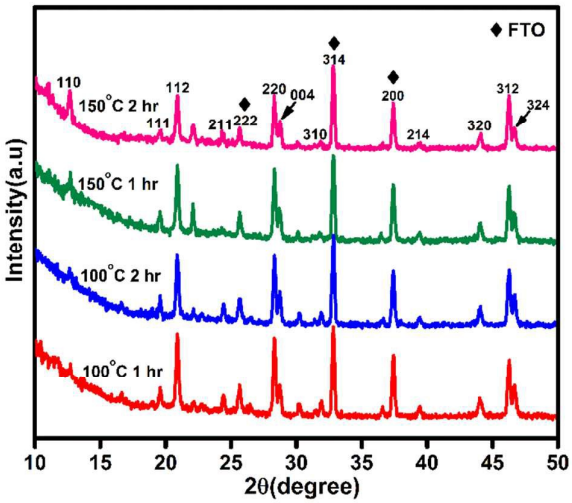

Figure 3. XRD spectra of $MAPbI_3$ thin films annealed at 100 °C and 150 °C for 60 and 120 minutes.

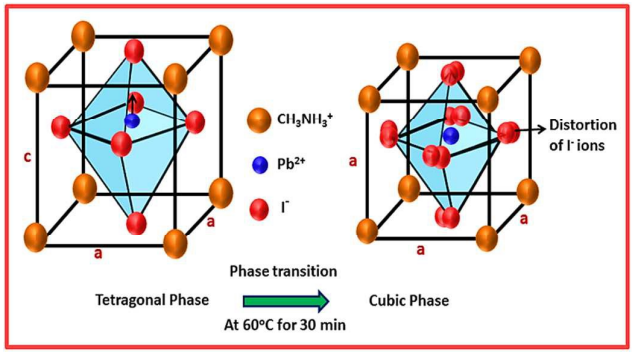

Figure 4. Graphical images of structural transformation of $MAPbI_3$ perovskite from tetragonal to cubic phase.

The tetragonal symmetry has been distorted only along one preferential axis which changes the unit cell dimensions and generates more diffraction lines as well as shift in its peak positions. The average grain sizes were calculated using Scherrer's formula (Equation (A) in supplementary)[22-24] and are 36.0, 39, 47.7, 59.1 nm respectively for 10, 30, 60 and 120 minutes annealed films at 60 °C.

3.2 Optical and morphological studies

UV-visible spectroscopy studies were carried out to investigate thermal effects on electronic band gap of $MAPbI_3$ thin films. Figure 5 (a) shows the absorption spectra of $MAPbI_3$ thin films annealed for 10 minutes at different temperatures. The exciton state in the organic–inorganic interface of $MAPbI_3$ is mainly associated with the bandgap of the inorganic layers which deliver a sharp peak even at RT.[25, 26] The absorption spectra exhibits a very wide spectral response over the entire visible range and the exciton peak appeared in the range of 400 - 450 nm and onset of absorption is between 700 - 800 nm. Figure 5 (b) shows the absorption spectra of films annealed at 60 °C for 10, 30, 60 and 120 minutes to further examine the variation of the band gap. The Figure S1 shows the UV-Visible spectra of $MAPbI_3$ perovskite annealed at 100 °C and 150 °C for 1 and 2 hours and shows a very little influence on absorption and band gap energy. It is observed that the absorption onset shifts towards the longer wavelength region with increased annealing temperature and time. The reduced optical bandgap energy with respect to annealing temperature and time is because of the increased grain size.[27, 28] The band gap of the $MAPbI_3$ films were estimated from absorption spectrum fitting (ASF) method[29, 30] where the absorption coefficient as a function of wavelength (λ) is,

$$\alpha(\lambda) = B(hc)^{m-1}\lambda\left(\frac{1}{\lambda}-\frac{1}{\lambda_g}\right)^m \qquad (1)$$

Here, λ_g, c, and h are wavelength corresponding to the optical bandgap, velocity of light and Planck's constant, respectively.
Using Beer-Lambert's law in equation (1),

$$Abs(\lambda) = B_1\lambda\left(\frac{1}{\lambda}-\frac{1}{\lambda_g}\right)^m + B_2 \qquad (2)$$

Here $B_1 = \left(B(hc)^{m-1}\times\frac{d}{2.303}\right)$ and B_2 are the constants

Equation 2 was used to estimate the bandgap by ASF method without the need of film thickness. The value of band gap in eV, can be calculated from the parameter λg using,

$$E_{gap}^{ASF} = \left(\frac{1239.83}{\lambda_g}\right) \qquad (3)$$

The λg value can be calculated from Figure 6(a-d) by extrapolating the linear region of $\left(\frac{A}{\lambda}\right)^{\frac{1}{m}}$ vs $\left(\frac{1}{\lambda}\right)$ curve at $\left(\frac{A}{\lambda}\right)^{\frac{1}{m}} = 0$.
Here m is the index which is ½ for direct bandgap.[31]

Figure 6 shows the band gap energy for the films prepared at RT and annealed at 60 °C, 100 °C, and 150 °C for 10 minutes and are 1.73, 1.66, 1.62, and 1.56 eV respectively. Figure S1 shows the perovskite films annealed at 100 °C and 150 °C for 1 and 2 hours with minor changes in the bandgap of 1.55, 1.53, 1.52, and 1.51 eV respectively. Upon annealing, the bandgap may also reduce due to the thermal vibrations of the organic (MA^+) crystal ions which weakly interact with the inorganic species (Pb) through the intermolecular hydrogen bonding occurring through the NH_3^+ group which predominantly reduce the surface energy of organic-inorganic interfaces.[32, 33] It is also suggested that longer annealing time increases the grain size by the agglomeration of grains at the surface of the film as confirmed in XRD and morphological analysis.

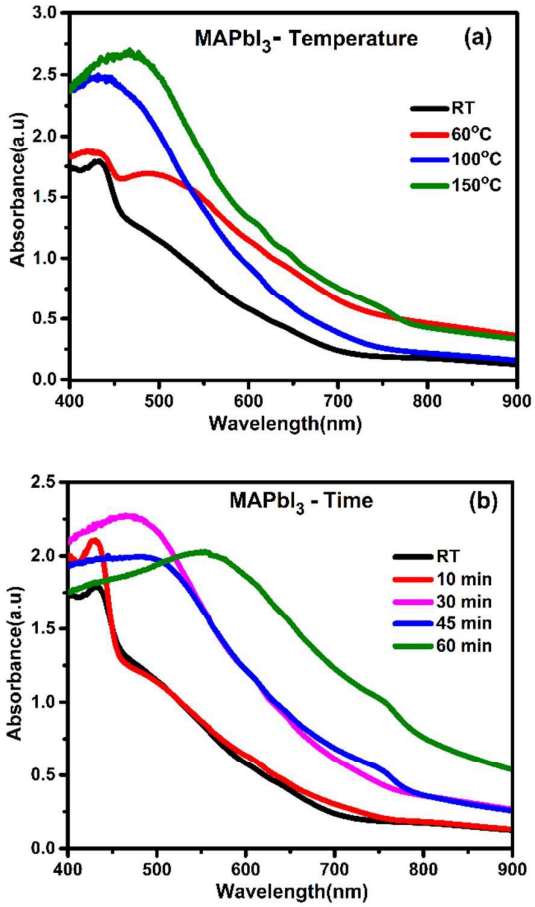

Figure 5. UV-Vis absorption spectra of $MAPbI_3$ thin films at (a) RT and annealed at 60 °C, 100 °C, and 150 °C for 10 minutes b) annealed at 60 °C for 10, 30, 60 and 120 minutes.

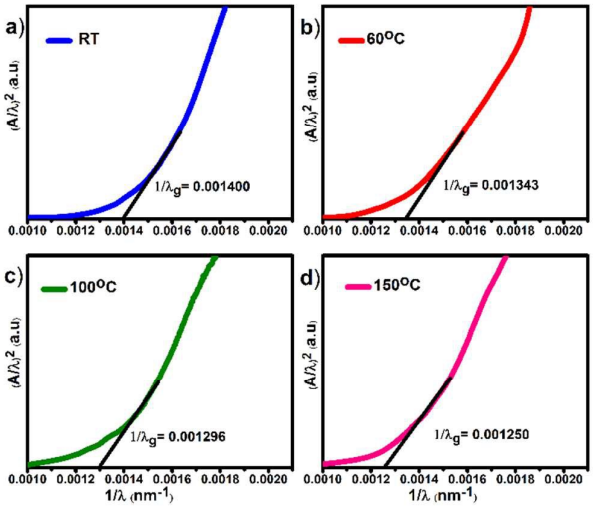

Figure 6. ASF plots for $MAPbI_3$ thin film at (a) RT and annealed at (b) 60 °C (c) 100 °C (d) 150 °C for 10 minutes.

The SEM images (Figure 7 (a-d)) depict the thermal effects on the surface morphology of the $MAPbI_3$ perovskite at RT and annealed at 60 °C, 100 °C and 150 °C for 10 minutes under ambient atmosphere. Instantly after spin coating, the film coverage is quite high with pinholes as shown in Figure 7(a). Upon annealing at 60 °C, the uniformity was condensed with decrease in number of pinholes and form tightly packed agglomerated grains at the surface until the crystallization is completed at the bottom layer of $MAPbI_3$. If the annealing temperature is increased to 100 °C, the size of the grains increased with voids in between due to agglomeration of small islands to become larger crystallites as is shown in Figure 7(c). The formation of still larger crystallites associated with voids in between is observed at 150 °C (Figure 7d). The change in surface morphology due to annealing is mainly caused by the excess surface energy gained from lattice which tends to increase the rate of perovskite crystallization at the organic-inorganic interfaces of $MAPbI_3$ in air.[34]

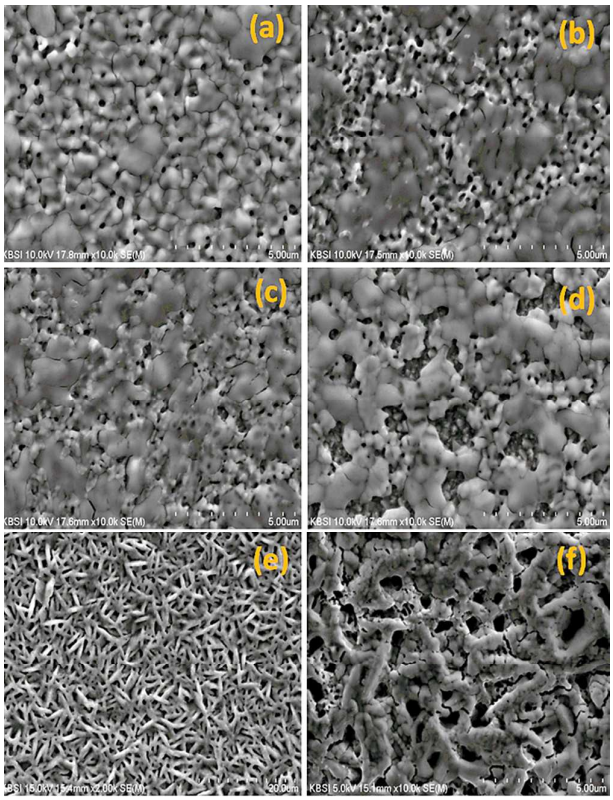

Figure 7. SEM images of MAPbI3 film at a) RT and annealed at b) 60 °C c) 100 °C d) 150 °C for 10 minutes and (e) 60 °C for 30 minutes (f) higher magnification image of (e)

The figure 7 (e-f) illustrates that the morphological transformation of $MAPbI_3$ perovskite from agglomerated crystals (Figure 7 e) to densely arranged needle like crystals. It is suggested that the change in annealing time facilitates the surface tension to upsurge the rate of perovskite crystallization by stretching the bonds at the surface of $MAPbI_3$ film.[35, 36] This extended surface energy may be minimized if the atoms have enough energy and time to diffuse to a lower energy nucleation sites.[37, 38] At low annealing temperature, large number of critical nucleation sites are formed that tends to form smaller crystallites and at higher annealing temperature result fewer nucleation sites roots to the formation of larger crystalline at the surface.

3.3 Surface analysis of $MAPbI_3$ Perovskites

The XPS spectra were recorded to investigate the interaction of organic-inorganic species in $MAPbI_3$ thin film and to understand the impact of annealing on elemental chemical states and relative surface elemental composition. The XPS survey spectra are shown in Figure S2. The small features at binding energies of 284.7, 401.0 and 531.0 eV corresponds to the photoelectron peaks of C 1s, N 1s, and O 1s respectively. The doublet peaks of I, Pb are located at 618, 137 eV respectively with spin orbit splitting.[39] The elemental surface composition of the $MAPbI_3$ is depicted in Figure S2.

3.3.1 High resolution X-ray photoelectron (HRXPS) spectra of $MAPbI_3$ thin films

High resolution XPS spectra were acquired over much restricted ranges to evaluate the thermal effects on different chemical states of the same element with the atomic concentration. Typically, the atomic concentration of the element was extracted from the core-level spectra using CASA XPS software using the average matrix relative sensitivity factors (AM-RSFs)[40, 41] equation B given in supplementary (Figure S3). XPS data fitted with Gaussian-Lorentzian (30 % Gaussian) functions and Shirley type background.[42] The core-level spectra of C 1s, O 1s, and N 1s for the $MAPbI_3$ perovskite at RT and annealed at 60 °C, 100 °C, and 150 °C for 10 minutes are shown in Figure 9(a-l). The deconvoluted characteristics of carbon peaks exhibited the bound state of carbon species with atmospheric oxygen, shown in Figure 8(a-d). At RT, the peak at 283.17 eV assigned to the aliphatic hydrocarbon (C-H/C-C) and the peak at 283.97 eV corresponds to hydroxyls (C-O). The next higher binding energy peak at 284.84 eV corresponds to the carbon atoms bonded with single nitrogen atoms (C-N). The carbon adjacent to (C=O) is the most electron withdrawing environment that corresponds to the peak at 285.81.[43] This distortion causes the variation of atomic concentration of C 1s components and is given inset in Figures 8(a-d).

The hygroscopic nature of $MAPbI_3$ thin films were subjected to the surface oxidation when exposed to air. Figure 8(e-h) show the O 1s core levels spectra deconvoluted into five oxygen binding states located at 530.51, 531.17, 532.06, 532.16 and 533.22 eV come from weakly adsorbed O molecules in air, hydroxyls (C-O), carbonyls (C=O), (C-OH) and aliphatic O-C-O respectively for RT and annealed at 60 °C, 100 °C, and 150 °C. It is found that $MAPbI_3$ films drastically affected by surface oxidation resulted from the chemisorbed or dissociated oxygen species. It is clear that the variation in atomic percentage of O 1s is mainly attributed to the elimination of weakly bonded organic components at higher annealing temperature.[44] The reduction of chemisorbed O and carbonyl (C-O) species at 150 °C lead to appear O-C=O and O=C-N species at higher binding energy range of 534.64 and 535.42 eV respectively. Figure 8(i-l) shows the XPS N 1s core levels spectra of $MAPbI_3$ films at RT and annealed at 60 °C, 100 °C, and 150 °C for 10 minutes. At RT, the N 1s deconvoluted to three spectral contributions such as single and double bounded nitrogen atoms with carbon atoms (N-C,N=C) and amide ions ($-NH_2$) located at the binding energies 398.70, 398.92, and 399.31 eV respectively.[45] The appearance of amide group (N-C=O) is thermodynamically favourable at 100 °C and 150 °C.

The doublet orbitals of Pb ($4f_{7/2}$ and $4f_{5/2}$) and I ($3d_{3/2}$ and $3d_{5/2}$) are quantified with an area ratio of 3:4 and 2:3 and elemental spin orbit splitting (SOS) of 11.5 and 4.8 was fixed respectively with an equal FWHM.

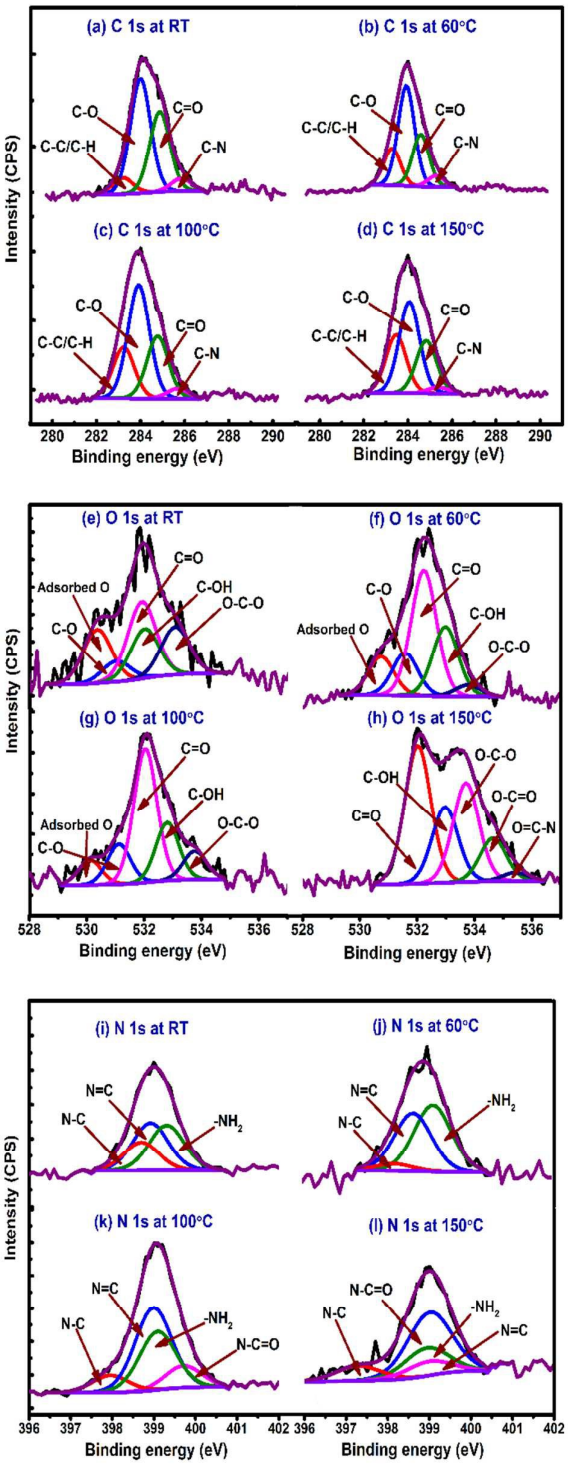

Figure 8. XPS Core-level spectra of (a-d) C 1s, (e-h) O 1s, and (i-l) N 1s for the $MAPbI_3$ thin films at RT and annealed at 60 °C, 100 °C, and 150 °C for 10 minutes in air.

Prior to peak fitting Pb and I, the transition intensity is measured using two independent quantification regions to avoid the creation of poor background with high residues. Figure 9 (a-d) show the

deconvoluted XPS spectra of I 3d doublets respectively of $3d_{5/2}$ are at 619.5 and 631 eV corresponds to I_3^- charge state and $3d_{3/2}$ are at 619.37 and 630.87 corresponds to the I_2^+ charge state. Figure 9 (e-h) show the Pb core-level doublet spectra respectively of $4f_{7/2}$ are at 138.0 and 142.8 eV corresponds to the metallic lead (Pb) and $4f_{5/2}$ peaks are at 137.7 and 142.5 eV corresponds to Pb (II).[46] The significant change in the surface states of Pb 4f core levels indicates that the surface re-structuring of Pb atoms into Pb ions with oxygen states upon annealing. Particularly, the Pb (II) species percentage is relatively higher than the metallic Pb even while increasing the temperature up to 150 °C, which illustrates that the Iodine species strongly interact with Pb species and forms donor-acceptor complex (Pb-I charge transfer interface) between the iodine atoms and Pb atoms.[47] The internal charge transfer occur between the valence states of Pb and iodine (I) atoms such as, the low electronegative (Pauling scale 1.87) Pb atom donates its excess unpaired electrons (outermost p subshells) to the high electronegative (Pauling scale 2.66) iodine (I). During the electrons transfer process, the Pb gets oxidized to attain its oxidation state +2 such as Pb^{2+} ion and iodine reduced as iodide ion ($2I^-$). The remaining unpaired electrons in the 4f valence levels (outermost s subshells) of Pb atoms have either parallel or anti-parallel orientation to the orbital angular momentum that causes the energy difference in the Pb 4f valence states.

Figure 10 (a-c) shows that the HRXPS spectra of C 1s, O 1s, and N 1s singlet for $MAPbI_3$ perovskite annealed at 60 °C for 30 minutes. The estimation of binding states with its atomic concentration is a significant aspect of revealing the thermal effects on $MAPbI_3$ perovskite in XPS spectra. Figure 10 (a) C 1s core-levels spectra of 30 minutes annealed at 60 °C exhibited additional binding states due to epoxy carbon (C-O-C) and carboxylate carbon (O-C=O) at 288.03 and 289.33 eV respectively compared to 10 minutes annealed film (Figure 8(b). [46] The increase in annealing time could incorporate additional oxygen free radicals to the carbon species that shift the binding energy positions. Moreover, Figure 10 (b) shows the O 1s spectra with additional peaks due to lattice oxygen (O^{2-}), iodate (IO_3^-) and carboxylates (O-C=O) at the binding energy of 528.44, 529.95 and 534.76 eV respectively. It is suggested that the hygroscopic methylammonium cation could have strongly bonded with the oxygen than metal-halide (Pb-I) complex under atmospheric conditions in 10 minutes annealed films. In addition, the ionic radii of organic cation are much larger than inorganic lead and halide anions and hence, increase in annealing time might have led to the delocalization of halide free radicals which directly bond to the surface oxygen atoms.[48] The noticeable shift in the O 1s maxima could be due to the incorporation of additional oxygen atoms into the distorted lattice of metal-halide complex. On the other hand, the N 1s core level spectra (Figure 10 c) exhibited distinguished binding states of amide carbonyl (N-C=O) at 398.60 eV and nitrogen single bonded with oxygen atoms (N-H) at 397.24 eV might be arising from dehydrogenated NH_2 binding states.[46]

The core-level 4f spectrum of Pb for the $MAPBI_3$ films annealed at 60 °C for 30 minutes is shown in Figure 11 (b) with additional two doublets associated to metallic lead (Pb (0)) at 137.77, 142.65 eV and oxidised lead(II) at 138.20 and 143.08 eV.[46] The unsaturated Pb reveals the metallic characteristics of lead and indicates the deficiency of iodide species in the perovskite lattice; the metallic lead species in the 10 minutes annealed film could acts as a recombination centres.[49] Increase in annealing time further oxidize the Pb 4f species and is confirmed by the existence of lead monoxide (PbO) at 144.25 eV (1.69%) and 137.05 eV (3.32%).

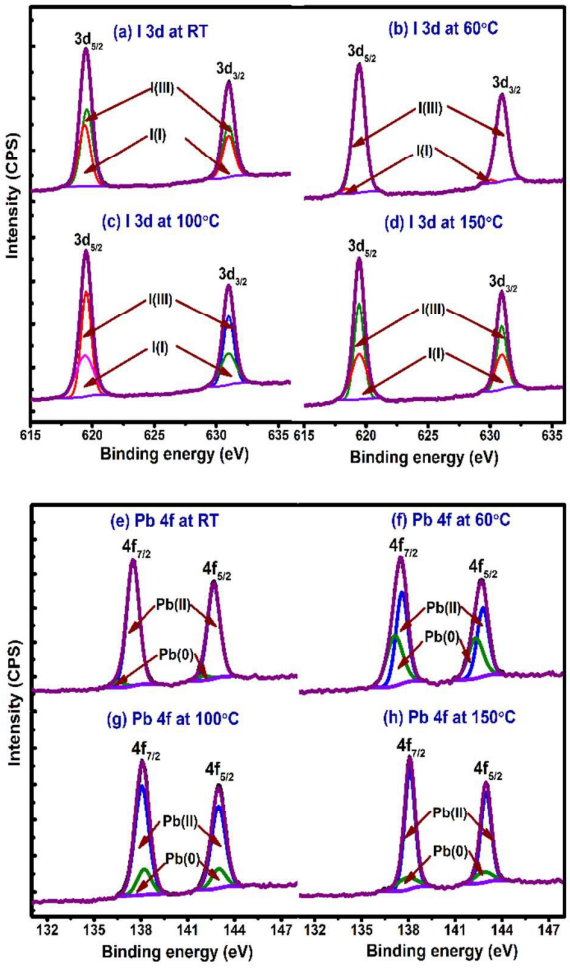

Figure 9. XPS core level spectra of (a-d) I 3d and (e-f) Pb 4f doublets for $MAPbI_3$ thin films at RT and annealed at 60 °C, 100 °C and 150 °C for 10 minutes.

The high resolution XPS spectra of I 3d (annealed at 60 °C for 30 min) is shown in Figure 11(a). Iodine exhibits very strong interaction with atmospheric oxygen since the doublets of $3d_{5/2}$ and $3d_{3/2}$ are deconvoluted into three distinguished valence states corresponding to iodide (I^-) at 629.33, 617.83 eV, triiodide (I^{3-}) at 619.01, 630.49 eV and iodate (IO^{2-}) anion at 620.20, 631.81 eV respectively. The increase in annealing time increased the surface oxidation of iodine and lead to the formation of iodite (IO_2^-) anion and the I_2^+ cation easily reduced to iodide (I^-) anion (Oxidation state of -1) in the $MAPbI_3$ perovskite film.[50]

4. Conclusion

In this work, we studied the impact of temperature on structural, morphology and optical properties of $MAPbI_3$ films with the help of complementary characterization techniques. $MAPbI_3$ thin films are optimized for low-temperature solution process preparations at the ambient atmospheric condition.

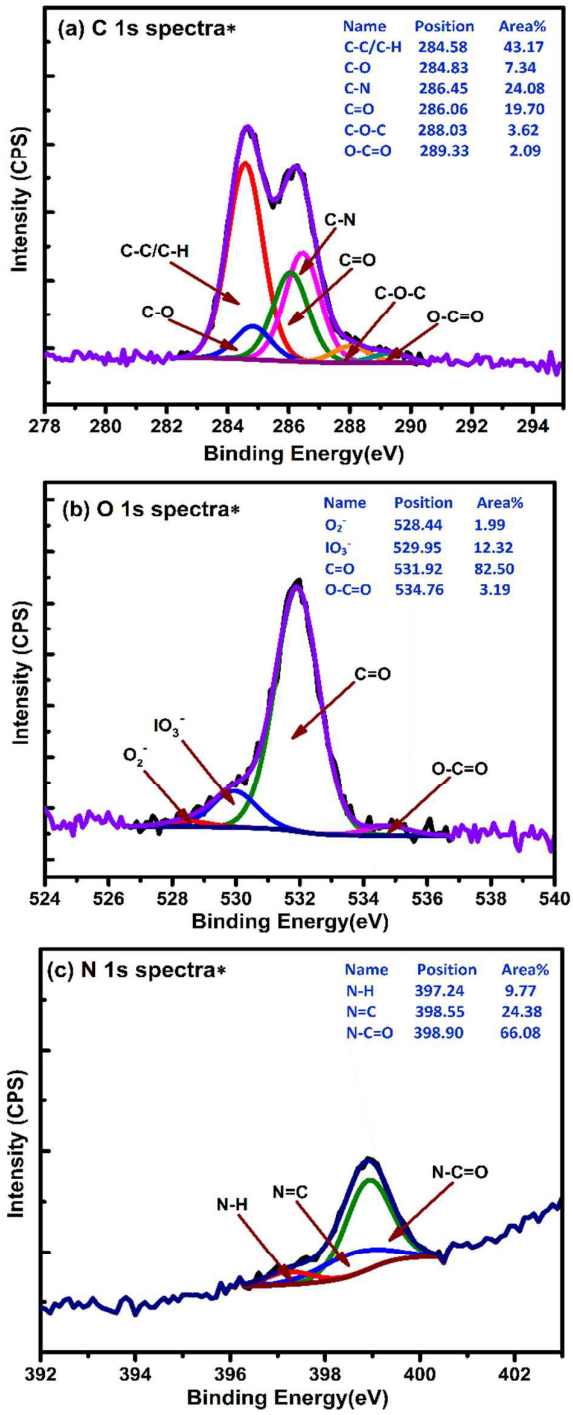

Figure 10. Core-level spectra of a) C 1s, b) O 1s, and c) N 1s for $MAPbI_3$ thin films annealed at 60 °C for 30 minutes.

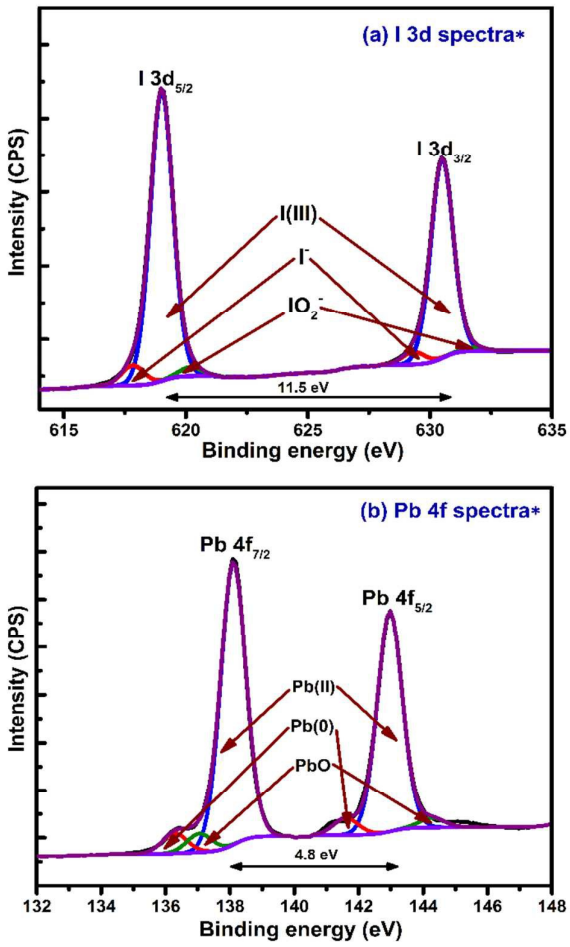

Figure 11. HRXPS core levels spectra of (a) I 3d and (b) Pb 4f for $MAPbI_3$ thin films annealed at 60 °C for 30 minutes.

Our findings are organized as follows, a) Structural transition from tetragonal to cubic of $MAPbI_3$ films occurred at 60 °C, b) The transformed cubic structure is highly preserved even when annealing temperature is elevated up to 150 °C, c) Larger aggregated grains are formed at the surface of $MAPbI_3$ films at higher annealing temperature and time, d) Changing the annealing time results in distinct morphological variance of $MAPbI_3$ films and e) The variations in binding states with atomic concentration of C 1s, N 1s, O 1s states and I 3d, and Pb 4f doublets states according to annealing temperature were clearly quantified from the XPS core-level spectra. The optimization of $MAPbI_3$ precursor concentration, solution temperature and spin speed would help to get uniform and stable perovskite film on FTO substrate at ambient atmosphere. It is suggested that annealing temperature of 60°C for 30 minutes is superior to ensure the perovskite crystallization. We conclude that these results offer a feasible way to achieve the better uniformity of $MAPbI_3$ films under atmospheric conditions. This initial effort is to comprehend the physical properties of $MAPbI_3$ thin films and to reveal the challenges associated with the processing of $MAPbI_3$ films in atmosphere. Further devices development and characterizations are under study to get highly efficient perovskite solar cells fabricated in atmospheric conditions without organic hole conducting material to get good stability.

Acknowledgements

This work was supported by Basic Science Research Program through the National Research Foundation of Korea (NRF) grant funded by the Korea government (No.2014005051).

Notes and references

1. M. A. Green, *Solar energy*, 2003, 74, 181-192.
2. E. Garnett and P. Yang, *Nano letters*, 2010, 10, 1082-1087.
3. B. O'regan and M. Grätzel, *nature*, 1991, 353, 737-740.
4. I. J. Kramer and E. H. Sargent, *Chem. Rev.*, 2013, 114, 863-882.
5. G. Li, R. Zhu and Y. Yang, *Nature Photonics*, 2012, 6, 153-161.
6. J. A. Chang, J. H. Rhee, S. H. Im, Y. H. Lee, H.-j. Kim, S. I. Seok, M. K. Nazeeruddin and M. Gratzel, *Nano letters*, 2010, 10, 2609-2612.
7. N.-G. Park, *The Journal of Physical Chemistry Letters*, 2013, 4, 2423-2429.
8. M. A. Green, A. Ho-Baillie and H. J. Snaith, *Nature Photonics*, 2014, 8, 506-514.
9. A. Kojima, K. Teshima, Y. Shirai and T. Miyasaka, *J. Am. Chem. Soc.*, 2009, 131, 6050-6051.
10. O. Malinkiewicz, A. Yella, Y. H. Lee, G. M. Espallargas, M. Graetzel, M. K. Nazeeruddin and H. J. Bolink, *Nature Photonics*, 2014, 8, 128-132.
11. N. J. Jeon, J. H. Noh, Y. C. Kim, W. S. Yang, S. Ryu and S. I. Seok, *Nature materials*, 2014.
12. D. Liu, J. Yang and T. L. Kelly, *J. Am. Chem. Soc.*, 2014, 136, 17116-17122.
13. Y. Zhou, M. Yang, A. L. Vasiliev, H. F. Garces, Y. Zhao, D. Wang, S. Pang, K. Zhu and N. P. Padture, *J. Mater. Chem.A*, 2015, 3, 9249-9256.
14. J.-H. Im, I.-H. Jang, N. Pellet, M. Grätzel and N.-G. Park, *Nature nanotechnology*, 2014, 9, 927-932.
15. J. Burschka, N. Pellet, S.-J. Moon, R. Humphry-Baker, P. Gao, M. K. Nazeeruddin and M. Grätzel, *Nature*, 2013, 499, 316-319.
16. Y. Zhao and K. Zhu, *The Journal of Physical Chemistry Letters*, 2013, 4, 2880-2884.
17. B. Culity and S. Stock, *Reading: Addition-Wesley*, 1978.
18. T. Supasai, N. Rujisamphan, K. Ullrich, A. Chemseddine and T. Dittrich, *Appl. Phys. Lett.*, 2013, 103, 183906.
19. T. Baikie, Y. Fang, J. M. Kadro, M. Schreyer, F. Wei, S. G. Mhaisalkar, M. Graetzel and T. J. White, *J. Mater. Chem.A*, 2013, 1, 5628-5641.
20. T. Oku, M. Zushi, Y. Imanishi, A. Suzuki and K. Suzuki, *Applied Physics Express*, 2014, 7, 121601.
21. R. Gottesman, E. Haltzi, L. Gouda, S. Tirosh, Y. Bouhadana, A. Zaban, E. Mosconi and F. De Angelis, *The Journal of Physical Chemistry Letters*, 2014, 5, 2662-2669.
22. P. Scherrer, *Nachrichten von der Gesellschaft der Wissenschaften zu Göttingen, mathematisch-physikalische Klasse*, 1918, 1918, 98-100.
23. J. I. Langford and A. Wilson, *J. Appl. Crystallogr.*, 1978, 11, 102-113.
24. D. Louër and N. Audebrand, *Adv. X-ray Anal*, 1999, 41, 556-565.
25. S. A. Kulkarni, T. Baikie, P. P. Boix, N. Yantara, N. Mathews and S. Mhaisalkar, *J. Mater. Chem.A*, 2014, 2, 9221-9225.
26. P. Umari, E. Mosconi and F. De Angelis, *Scientific reports*, 2014, 4.
27. B. J. Foley, D. L. Marlowe, K. Sun, W. A. Saidi, L. Scudiero, M. C. Gupta and J. J. Choi, *Appl. Phys. Lett.*, 2015, 106, 243904.
28. N. S. Pesika, K. J. Stebe and P. C. Searson, *The Journal of Physical Chemistry B*, 2003, 107, 10412-10415.
29. N. Ghobadi, *International Nano Letters*, 2013, 3, 1-4.
30. N. Serpone, D. Lawless and R. Khairutdinov, *The journal of Physical Chemistry*, 1995, 99, 16646-16654.
31. D. Souri and K. Shomalian, *J. Non·Cryst. Solids*, 2009, 355, 1597-1601.
32. K. O'Donnell and X. Chen, *Appl. Phys. Lett.*, 1991, 58, 2924-2926.
33. J. Tauc and A. Menth, *J. Non·Cryst. Solids*, 1972, 8, 569-585.
34. J. H. Noh, S. H. Im, J. H. Heo, T. N. Mandal and S. I. Seok, *Nano letters*, 2013, 13, 1764-1769.
35. Y. Zhao, A. M. Nardes and K. Zhu, *Faraday Discuss.*, 2015, 176, 301-312.
36. L. Etgar, P. Gao, Z. Xue, Q. Peng, A. K. Chandiran, B. Liu, M. K. Nazeeruddin and M. Grätzel, *J. Am. Chem. Soc.*, 2012, 134, 17396-17399.
37. G. E. Eperon, V. M. Burlakov, P. Docampo, A. Goriely and H. J. Snaith, *Advanced Functional Materials*, 2014, 24, 151-157.
38. M. Graetzel, R. A. Janssen, D. B. Mitzi and E. H. Sargent, *Nature*, 2012, 488, 304-312.
39. M. Seah and W. Dench, *Surface and interface analysis*, 1979, 1, 2-11.
40. M. Seah and I. Gilmore, *Physical Review B*, 2006, 73, 174113.
41. S.Hofmann, *Auger- and X-Ray Photoelectron Spectroscopy in Materials Science*, Springer, Berlin Heidelberg, 2013.
42. J. Kirz and D. Attwood, *X-RAY DATA BOOKLET*, 1986, 13.
43. J. You, Z. Hong, Y. M. Yang, Q. Chen, M. Cai, T.-B. Song, C.-C. Chen, S. Lu, Y. Liu and H. Zhou, 2014.
44. S. R. Raga, M.-C. Jung, M. V. Lee, M. R. Leyden, Y. Kato and Y. Qi, *Chemistry of Materials*, 2015, 27, 1597-1603.
45. T.-W. Ng, C.-Y. Chan, M.-F. Lo, Z. Q. Guan and C.-S. Lee, *J. Mater. Chem.A*, 2015, 3, 9081-9085.
46. C. Wagner, A. Naumkin, A. Kraut-Vass, J. Allison, C. Powell and J. Rumble Jr, *National Institute of Standards and Technology: Gaithersburg, MD*, 2003, 20899.
47. B. Conings, L. Baeten, C. De Dobbelaere, J. D'Haen, J. Manca and H. G. Boyen, *Advanced Materials*, 2014, 26, 2041-2046.
48. C. Elschenbroich and A. Salzer, *Organometallics: a concise introduction*, Vch Weinheim, 1989.
49. W. Zhang, S. Pathak, N. Sakai, T. Stergiopoulos, P. K. Nayak, N. K. Noel, A. A. Haghighirad, V. M. Burlakov, A. Sadhanala and W. Li, *Nature communications*, 2015, 6.
50. S. Leach, *The Journal of Physical Chemistry*, 1988, 92, 5373-5379.

